Design and Modulation Optimization of an MMC Based Braking Chopper

Viktor Hofmann, Patrick Hofstetter
SIEMENS AG
Vogelweiherstr. 1-15
Nuremberg, Germany
Tel.: +49 / 162 – 691 6655
E-Mail: viktor.hofmann@siemens.com
URL: http://www.siemens.com

Keywords

«Modular Multilevel Converters (MMC)», «Braking Chopper», «High voltage power converters», «Medium voltage», «Industrial application».

Abstract

This paper investigates MMC based braking chopper configurations with a centralized resistor. It analyzes, optimizes and compares different cell configurations and modulation methods. A detailed description of the limiting factors and boundary conditions as well as the available degrees of freedom are provided and the theoretical derivations are validated by simulation.

Introduction

The Modular Multilevel Converter (MMC) [1] is a well-suited converter topology for medium- and high-voltage applications, which provides a lot of features such as high output voltage quality, efficiency and easy scalability [2] – [4]. In medium-voltage applications, it is often used as an adjustable-speed motor drive for large-capacity fans or compressors [5], [6]. In high-voltage direct current (HVDC) applications, the MMC can be utilized e.g. to connect offshore wind parks to the onshore grid [7], [8].

In both application fields, the systems often require the capability of dynamic braking. In case of a variable speed drive, the dynamic braking is primarily used for emergency purposes. Furthermore, it is more cost effective than regenerative braking [9] or applied when there is no possibility of regenerative braking [10]. In general, this is the case when a diode rectifier is used as the front-end inverter (Fig. 1(a)). In HVDC applications, the system configuration typically consists of two back-to-back VSC terminals (Fig. 1(b)). These common system configurations are illustrated in Fig. 1. For the discussed connection of wind parks, it is necessary that the system applies to the grid code requirements. The AC grid voltage may drop for several periods and disable the capability of regenerative braking. It is essential to dissipate the generated wind power during this time to avoid DC overvoltage or even major system damages.

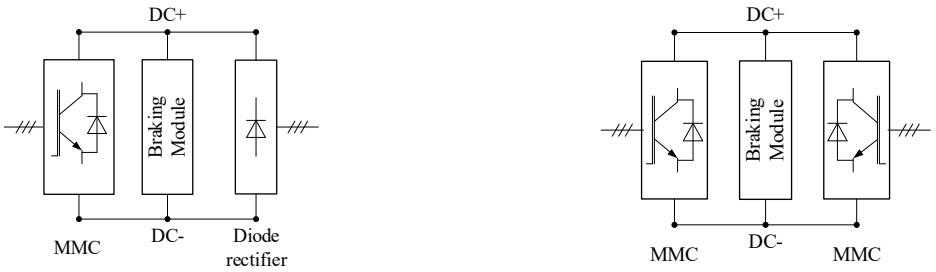

(a) MMC with diode front-end (b) Back-to-back MMC

Fig. 1: Typical system configurations of a braking application

The braking module is usually installed on the DC side between the terminals DC+ and DC-. There are several chopper topologies, which provide different advantages and disadvantages. The most common types are shown in Fig. 2. The classic way to realize a braking chopper, is the series connection of an IGBT and a braking resistor with a parallel diode (Fig. 2(a)). For higher system voltages, the IGBTs and diodes have to be designed as several series connected semiconductors. The power dissipation is performed by switching all semiconductors simultaneously in a two-level PWM operation, where the full DC-link voltage is applied across the chopper resistor. This topology offers a very simple design and control. The drawbacks are the very high dv/dt and di/dt as well as a bad EMI performance.

To reduce dv/dt and di/dt, modular chopper topologies were proposed, which offer a strictly modular design and good scalability [11, 12]. The main difference is the implementation of the chopper resistor. One possibility is to use a series connection of common MMC submodules (SM), such as half bridges (HB) and full bridges (FB), in series to a braking resistor (Fig. 2(b)). In this case, there is a single lumped resistor, which can be mounted outdoor and supplied by an air cooling.

Another solution is to distribute the braking resistor into the SMs. Typically, this option needs a water cooling and usually, the resistors cannot be mounted separately from the cell. It requires a special cell design and is challenging in diverting the high amount of generated heat. A possible design of such an SM is illustrated in Fig. 2(c). There are a lot of different cell designs. For example, it is possible to realize the switches 1 and 2 as passive components or the switch 3 as a single IGBT without an antiparallel diode to reduce the semiconductor effort. Furthermore, investigations were performed to combine the distributed resistor SM with a lumped resistor to reduce the SM cooling effort and increase the system performance [12].

The various topologies have different design criteria and operation modes. The general advantages and disadvantages were analyzed in [13]. This paper focuses on the topology shown in Fig. 2(b). A sinusoidal modulation method and an investigation on aspects of semiconductor utilization was presented in [14]. This paper focuses on the optimum design for different operation points. It considers the usage of only half bridges (HB) and full bridges (FB) within the braking chopper as well as a combination of both submodules (HB + FB) within a MMC braking chopper. Furthermore, it investigates the usage of different modulation methods, such as a superimposed higher frequency sinusoidal or a trapezoidal modulation. The derived optima will be validated by simulations.

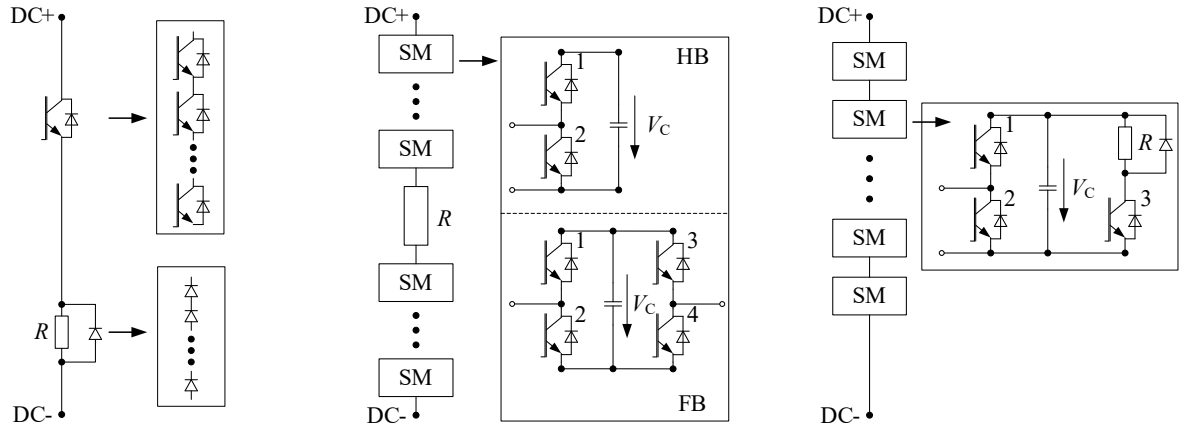

(a) Classic two level (b) MMC based with lumped resistor (c) MMC based with distributed resistors

Fig. 2: DC chopper topologies

Functional Principle

The considered MMC based braking chopper topology is illustrated in Fig. 2(b) and the functional principle will be explained by means of the equivalent circuit diagram shown in Fig. 3. The series connection of submodules can be seen as an adjustable voltage source. v_{Br} describes the modulated voltage of the braking chopper submodules and $v_{\mathrm{Arm},x\mathrm{p/n}}$ represents the modulated arm voltages of the positive (p) and negative (n) MMC arm, respectively, in a phase x. L_{Arm} is the arm inductance and R_{Arm} summarizes all resistive parts of an MMC arm.

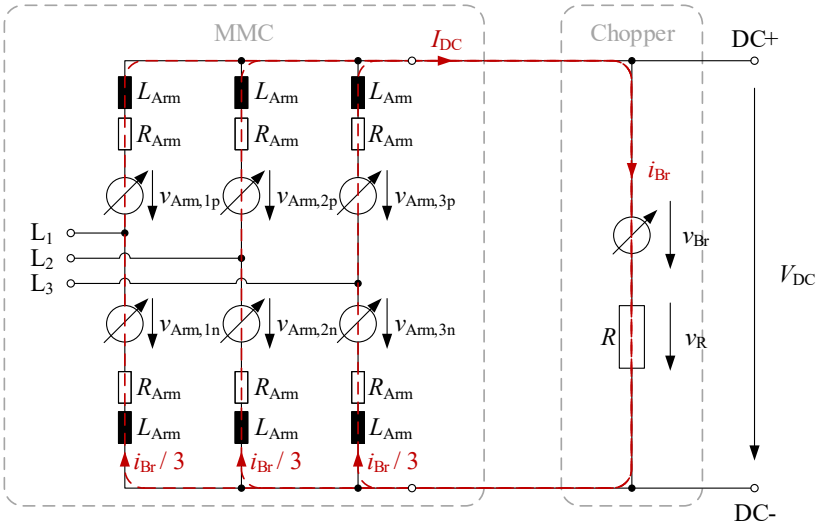

Fig. 3: Equivalent circuit diagram of MMC based braking chopper

In idle mode, the braking chopper modulates the DC voltage $v_{\mathrm{Br}} = V_{\mathrm{DC}}$ and there is no current flow through the braking resistor ($i_{\mathrm{Br}} = 0$). Due to zero-current switching, the losses are neglectable during this operation.

During active chopper operation, the dissipation power is controlled by the DC current component $i_{\mathrm{Br,DC}}$ of the chopper current i_{Br}. It is assumed that the total power which results from the MMC is dissipated by the braking resistor. Consequently, the DC component of the chopper current is equal to the MMC DC current I_{DC} and the dissipated power P_{Br} is given by:

$$P_{\mathrm{Br}} = V_{\mathrm{DC}} \cdot i_{\mathrm{Br,DC}} = R \cdot i_{\mathrm{Br,rms}}^2 \tag{1}$$

$$i_{\mathrm{Br,DC}} = I_{\mathrm{DC}} \tag{2}$$

Furthermore, it is necessary to ensure that the net energy flow to the cell capacitors $\overline{e_{\mathrm{Br}}}$ is zero:

$$\overline{e_{\mathrm{Br}}} = \int_0^{2\pi} (v_{\mathrm{Br}} \cdot i_{\mathrm{Br}}) \mathrm{d}\omega t = 0 \tag{3}$$

Therefore, an AC current is modulated, which circulates between the MMC and the braking chopper. In this paper, three different AC current profiles are considered: a sinusoidal current (1H), a sinusoidal current that is additionally superimposed with a third harmonic (3H) and a trapezoidal current (TR). Consequently, the AC current component is given by:

$$i_{\mathrm{Br,AC,1H}} = \hat{I}_{\mathrm{AC}} \cdot \sin(\omega t) \tag{4}$$

$$i_{\mathrm{Br,AC,3H}} = \hat{I}_{\mathrm{AC}} \cdot (\sin(\omega t) + 1/6 \sin(3\omega t)) \tag{5}$$

$$i_{\mathrm{Br,AC,TR}} = \begin{cases} \frac{\mathrm{d}v/\mathrm{d}t}{R\cdot 2\pi f}\cdot \omega t & 0 \le \omega t < \tau \\ \hat{I}_{\mathrm{AC}} & \tau \le \omega t < \pi - \tau \\ -\frac{\mathrm{d}v/\mathrm{d}t}{R\cdot 2\pi f}\cdot (\omega t - \pi) & \pi - \tau \le \omega t < \pi + \tau \\ -\hat{I}_{\mathrm{AC}} & \pi + \tau \le \omega t < 2\pi - \tau \\ \frac{\mathrm{d}v/\mathrm{d}t}{R\cdot 2\pi f}\cdot (\omega t - 2\pi) & 2\pi - \tau \le \omega t < 2\pi \end{cases} \quad \text{if} \quad , \quad \text{with } \tau = \frac{\hat{I}_{\mathrm{AC}}\cdot R\cdot 2\pi f}{\mathrm{d}v/\mathrm{d}t} \tag{6}$$

$\hat{I}_{\mathrm{AC}}$ describes the amplitude of the modulated current, $\mathrm{d}v/\mathrm{d}t$ the permissible voltage rise and f the modulated fundamental frequency. The resulting braking chopper current is finally given by:

$$i_{\mathrm{Br}} = i_{\mathrm{Br,DC}} + i_{\mathrm{Br,AC}} \tag{7}$$

The voltage drop across the resistor is given by Ohm's law and the modulated voltage of the braking chopper v_{Br} has to ensure a constant DC voltage between the terminals DC+ and DC– at any time:

$$v_{\mathrm{Br}} = V_{\mathrm{DC}} - R\cdot i_{\mathrm{Br}} \tag{8}$$

These equations clearly describe the braking chopper operation. The energy requirement of the chopper cells is fulfilled by adjusting the modulated AC current component. For a given system configuration and operation point, the AC amplitude of the modulated current is calculated by solving eq. (3) for the different modulation methods:

$$\hat{I}_{\mathrm{AC,1H}} = \sqrt{2\left(\frac{V_{\mathrm{DC}}\cdot I_{\mathrm{DC}}}{R} - I_{\mathrm{DC}}^2\right)} \tag{9}$$

$$\hat{I}_{\mathrm{AC,3H}} = \sqrt{\frac{72}{37}\left(\frac{V_{\mathrm{DC}}\cdot I_{\mathrm{DC}}}{R} - I_{\mathrm{DC}}^2\right)} \tag{10}$$

$$\hat{I}_{\mathrm{AC,TR}} = \frac{\mathrm{d}v/\mathrm{d}t}{8Rf}\cdot\left\{1 - 2\cos\left[\frac{1}{3}\left(\pi + \tan^{-1}\left(\frac{8f\sqrt{I_{\mathrm{DC}}\cdot R(V_{\mathrm{DC}} - I_{\mathrm{DC}}\cdot R)(48(R\cdot f\cdot I_{DC})^2 - 48V_{\mathrm{DC}}\cdot I_{\mathrm{DC}}\cdot R\cdot f^2 + (\mathrm{d}v/\mathrm{d}t)^2)}}{96(R\cdot f\cdot I_{DC})^2 - 96V_{\mathrm{DC}}\cdot I_{\mathrm{DC}}\cdot R\cdot f^2 + (\mathrm{d}v/\mathrm{d}t)^2}\right)\right)\right]\right\} \tag{11}$$

Exemplary voltage and current profiles are illustrated in Fig. 4 for different modulation methods.

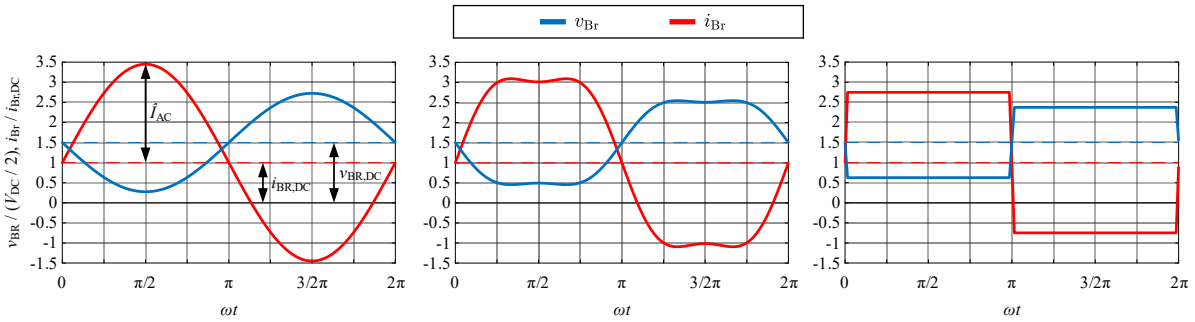

(a) Sinusoidal (b) Additional third harmonic (c) Trapezoidal

Fig. 4: Exemplary modulated fundamental voltage (blue) and current profiles (red) of the braking chopper for different modulation methods

Design optimization

In this section a design optimization is performed for different modulation methods and cell configurations of the braking chopper. Several limitations are discussed and the optimum point of operation is derived.

Theoretical operation area

An important issue is the power dissipation capability of the braking chopper, which can be described by the maximum admissible DC current. As the braking chopper can easily be scaled for higher voltage ratings by connecting several submodules in series, the performed analysis is not limited to any certain voltage level. There are several degrees of freedom and different limitations, which must be considered. The basic limitations depend on the used cell types as well as on the applied modulation method. For a given system, the possible operation area of the braking chopper can be described by the DC current and the specific resistance R_{Spec}:

$$R_{\mathrm{Spec}} = \frac{R}{V_{\mathrm{DC}}} \tag{12}$$

The various limitations will be discussed in the following. First, an MMC braking chopper is considered, which is only assembled with HB submodules and sinusoidal modulated. Since only a positive or zero voltage level can be modulated with half bridge cells, this topology is limited to a modulated chopper voltage that is always greater zero. The green hatched area in Fig. 5 shows the possible operation area of this topology, where I_{Nom} describes the nominal current rating of the applied semiconductors and is assumed to be $I_{\mathrm{Nom}} = 1400\mathrm{A}$.

The admissible operation area can be expanded, if at least a portion of full bridges is installed in the braking chopper. In this mixed cell configuration, it is important to pay attention to an energy balanced operation, because the HB can only be discharged during a negative cell current. In dependency of the operation point, a certain amount of full bridges must be available to ensure a stable operation [15]. The possible operation area of this mixed cell configuration (HB+FB) is limited by the red line in Fig. 5. At this point, the chopper current is always positive and the HB cannot be discharged anymore.

It is possible to shift both before mentioned limitations by using other modulation methods. An additional third voltage harmonic or the trapezoidal modulation expands the possible operation area of the HB chopper due to the lower absolute voltage level of the modulated chopper voltage (cf. Fig. 4 and eq. (1)-(11)). In contrast, the possible operation range of the mixed cell chopper configuration decreases, because of the reduced negative chopper current. The trapezoidal modulation leads to the same possible operation area of the HB and mixed cell braking chopper.

To enable an operation in the black hatched area, it is necessary to use bipolar submodules such as full bridges. FB are not limited by the before mentioned restrictions.

The black line marks the absolute limit of the considered operation principle for all braking chopper configurations. At this point, the DC current component of the braking chopper $i_{\mathrm{Br,DC}}$ causes a voltage drop across the braking resistor that is equal to V_{DC}. Consequently, no active voltage modulation must be performed by the braking chopper at this point and the total power is already dissipated completely by the DC component. Higher power ratings would require the modulation of a negative DC chopper voltage. This would lead to a non-constant DC terminal voltage V_{DC}, when it is attempted to ensure the energy balance in the chopper cells.

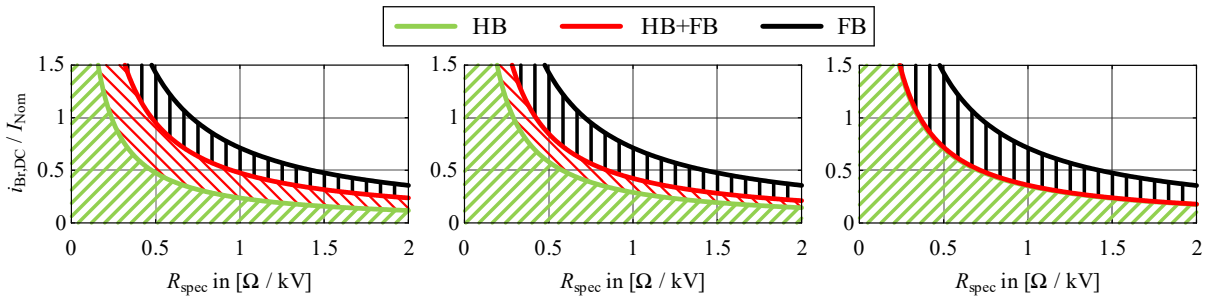

(a) Sinusoidal (b) Additional third harmonic (c) Trapezoidal

Fig. 5: Possible operation area of different cell configurations and different modulation methods

Partial load operation

Another important aspect is the partial load operation. The chopper must be able to operate at all partial load conditions. Therefore, a partial load factor a is introduced:

$$a = \frac{i_{\mathrm{Br,DC}}}{I_{\mathrm{DC}}} \tag{13}$$

$a = 1$ describes a full load operation as it was discussed before and $a = 0$ represents the idle mode. The maximum voltage level, which has to be modulated by the chopper arm, increases at lower partial load factors a (cf. eq. (1) – (11)). Fig. 6 illustrates the maximum modulated arm chopper voltage $V_{\mathrm{Br,Max}}$ for different modulation methods in dependence of the partial load factor a. The maximum modulated voltage level is an important design criterion and determines the minimum needed amount of cells. The maximum modulated voltage level can be reduced by using a trapezoidal modulation. This reduces the hardware effort and consequently the total costs. This illustration is irrespective of the used cell type and also valid for the different current limits of the appropriate cell types according to Fig. 5. Increasing the partial load factor from $a = 0$ to $a = 1$ (Fig. 6) is equivalent to increasing the DC current from zero to the possible limit of the appropriate modulation method and cell configuration for a fixed resistance as it is depicted in Fig. 5.

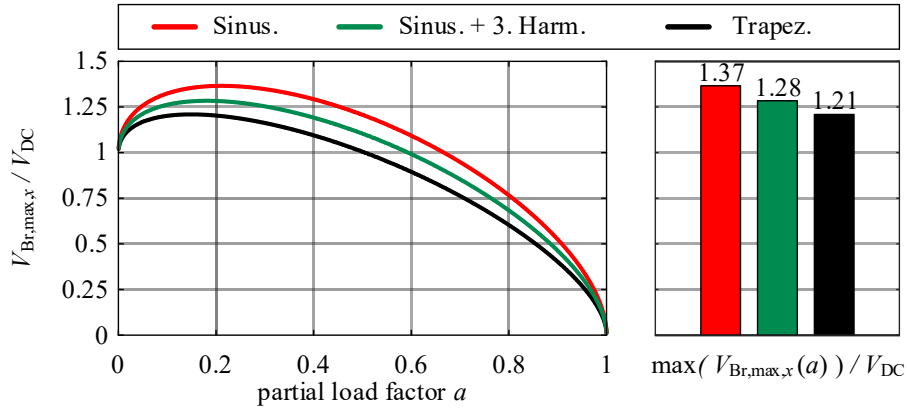

Fig. 6: Maximum modulated voltage level of a braking chopper in dependence of the partial load factor a.

Beside the total amount of cells, the cell capacitor sizing is a further design criterion. It is determined by the energy fluctuation e_{Br} and the resulting energy ripple ΔE_{Br}, respectively:

$$e_{\mathrm{Br}} = \int_0^{t'} (v_{\mathrm{Br}} \cdot i_{\mathrm{Br}}) \mathrm{d}\omega t \tag{14}$$

$$\Delta E_{\mathrm{Br}} = \max(e_{Br}) - \min(e_{Br}) \tag{15}$$

The dimensioning of the cell capacitors is also affected by the desired tolerance band of the submodules K_{T}. The energy fluctuation corresponds to a permissible cell voltage range. Consequently, the relationship between the submodule capacitance C_{m}, the energy ripple and the permissible voltage fluctuation as well as the nominal cell voltage $V_{\mathrm{C,0}}$ is specified by:

$$\frac{\Delta E_{\mathrm{Br}}}{N_{\mathrm{Br}}} = 2 K_{\mathrm{T}} C_{\mathrm{m}} V_{C,0}^2 \tag{16}$$

Fig. 7 illustrates the relative energy ripple for different cell types and modulation methods. The values are related to the modulation frequency f_{M} and the maximum power P_{Max}. This power is reached for a specific chopper configuration at full load operation $a = 1$ (cf. Fig. 5). Higher power ratings and lower modulation frequencies increase the absolute energy ripple accordingly.

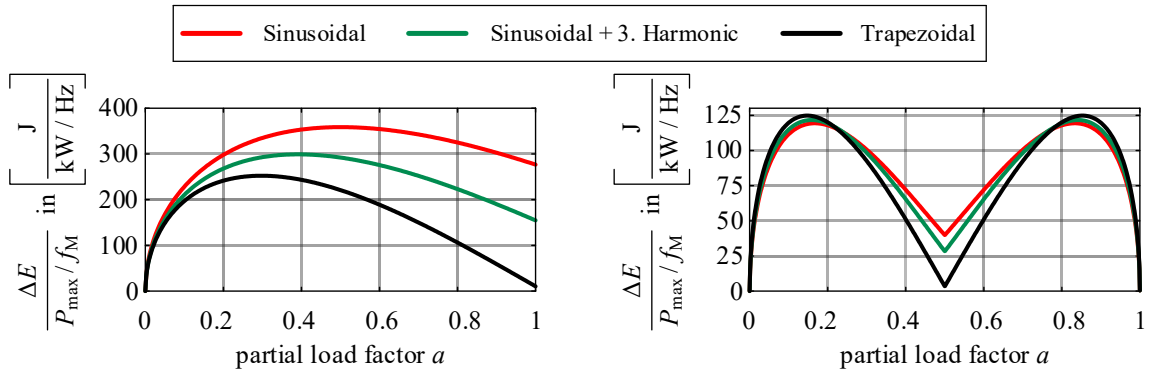

(a) HB braking chopper (b) FB braking chopper

Fig 7: Energy ripple in partial load operation for different cell types and modulation methods

The FB chopper configuration (Fig. 7(b)) offers the lowest energy ripple at a partial load factor $a = 0.5$. This operation is marked by the red line in Fig. 5(c), that also represents the absolute operation limit of the trapezoidal modulated HB and mixed cell configuration. At this point, the chopper voltage and current profiles modulate alternately the minimum values within a fundamental modulation period. A low energy ripple is also established at no load and full load operation (the full load operation is represented by the black line in Fig. 5). All modulation methods provide the same maximum power for a specific chopper configuration (cf. Fig. 5). The maximum energy ripple is approximately in the same range for all modulation methods.

For HB chopper configurations (Fig. 7(a)), the trapezoidal modulation method is beneficial in comparison to the sine-based variants. It provides the lowest relative energy ripple and consequently the highest utilization of the installed capacitors. Note, that the discussed modulation methods result in different maximum power values (cf. Fig. 5), when a HB chopper is considered.

Thermal admissible current

Another limitation is the thermal admissible current of the semiconductors. The thermal load is evaluated by calculating the semiconductor losses of the cells. This is performed by an average loss model according to [16], which offers a high accuracy for steady state operation. Afterwards, the junction temperature can be determined by means of a thermal model. Fig. 8 shows the resulting thermal limitation of a HB and a FB braking chopper for different modulation methods. The trapezoidal modulation increases the power dissipation capability significantly in comparison to a sinusoidal modulation (note, that the sinusoidal modulation method has its maximum at $R_{\mathrm{spec}} = 0.42\ \Omega/\mathrm{kV}$ and $i_{\mathrm{Br,DC}}/I_{\mathrm{Nom}} = 0.56$). For higher ratings of the specific resistor R_{spec}, the chopper operation is not limited by thermal issues.

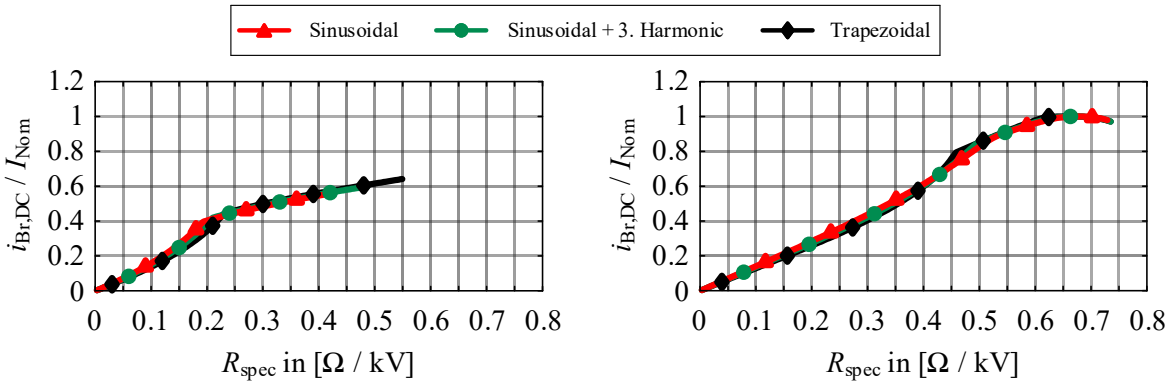

(a) HB braking chopper (b) FB braking chopper

Fig. 8: Thermal limitation of the HB and FB braking chopper for different modulation methods

Resulting operation area

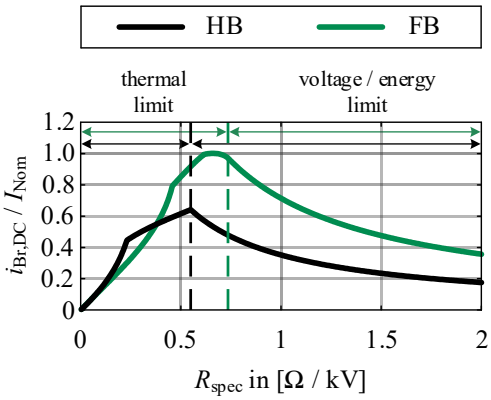

Fig 9: Resulting admissible operation area for a trapezoidal modulation method and different braking chopper configurations.

The analysis shows, that the trapezoidal modulation method is beneficial in several concerns. The half bridge cell type should be used for common power ratings and provides lower hardware costs. By assembling the braking chopper with full bridge submodules, it is possible to expand the possible operation area and realize higher power ratings. Fig. 9 shows an overview of the resulting admissible operation range for a trapezoidal modulation method and different braking chopper topologies. HB and FB chopper configurations are thermally limited for lower specific resistor values (dashed lines in Fig. 9). At higher resistor values, voltage and energy limitations delimit the braking chopper operation.

The most relevant design criteria were analyzed up to now. However, there are further issues in a real system configuration, such as a maximum admissible peak current of the semiconductors or the admissible rms current of passive and mechanical components (e.g. bus bars), that won't be discussed in this paper.

Simulation results

To verify the functionality of the proposed modulation method and validate the analysis, full scale simulation studies are performed. The investigated system is a grid connected back-to-back MMC configuration and the equivalent circuit diagram is illustrated in Fig. 10. The system design is based on typical medium voltage applications. Both grid sides operate at a $f_{\mathrm{G}} = 50$ Hz grid frequency and AC phase-to-phase voltages of $v_{\mathrm{sLI/II},x} = 11\mathrm{kV}$. The MMC DC voltage is set to $V_{\mathrm{DC}} = 18\mathrm{kV}$.

A HB chopper configuration is applied with $N_{\mathrm{Br}} = 20$ chopper cells. An exemplary design will be explained in the following. To ensure a sufficient voltage availability during partial load operation (cf. Fig. 6), the nominal cell voltage is set to $V_{\mathrm{C},0} = 1.1\mathrm{kV}$. A $C_{\mathrm{m}} = 5$ mF submodule capacitance is chosen. In this way, the braking chopper and all MMC arms are equipped with the same amount of cells and also with the same cell type. By evaluating eq. (16), the chopper submodule capacitance can be further reduced.

According to Fig. 9, the highest chopper power is achieved at a specific resistor $R_{\mathrm{spec}} = 0.549\,\Omega/\mathrm{kV}$. This leads to an absolute resistance $R_{\mathrm{Br}} = 9.882\,\Omega$ with a maximum admissible DC current $i_{\mathrm{Br,DC}} = 898\,\mathrm{A}$ and the maximum power $P_{\mathrm{max}} = 16.16\,\mathrm{MW}$, respectively. Various operating scenarios are performed to verify different operation modes. The simulated operation sequence is illustrated in Table I. Fig. 11 shows the simulation results.

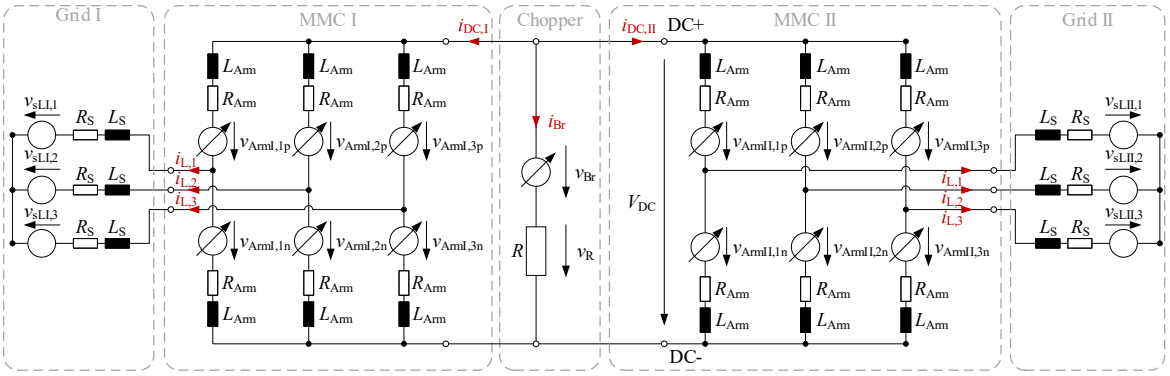

Fig. 10: Equivalent circuit diagram of the simulated system.

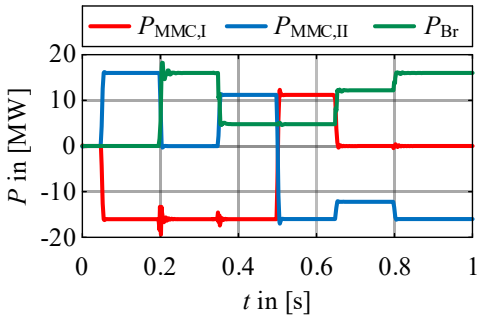

(a) Load profiles

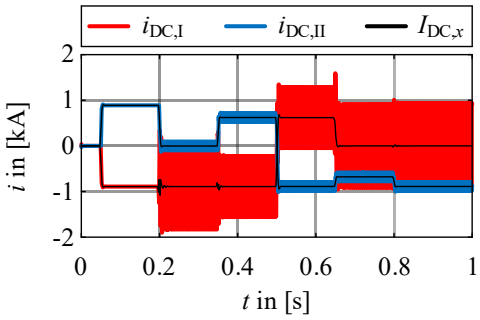

(b) DC currents

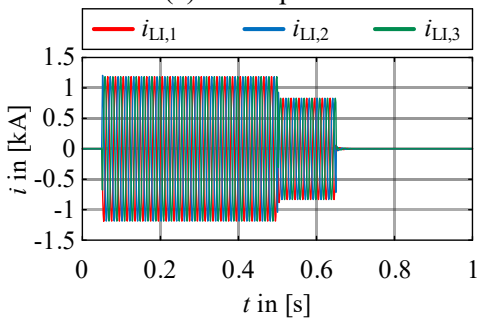

(c) Phase currents MMC I

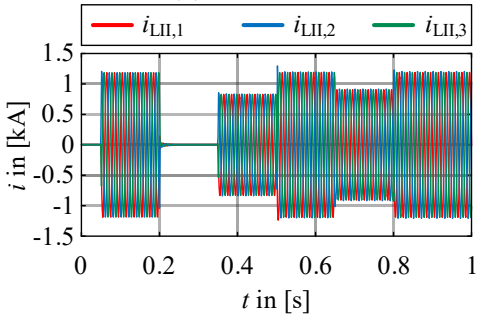

(d) Phase currents MMC II

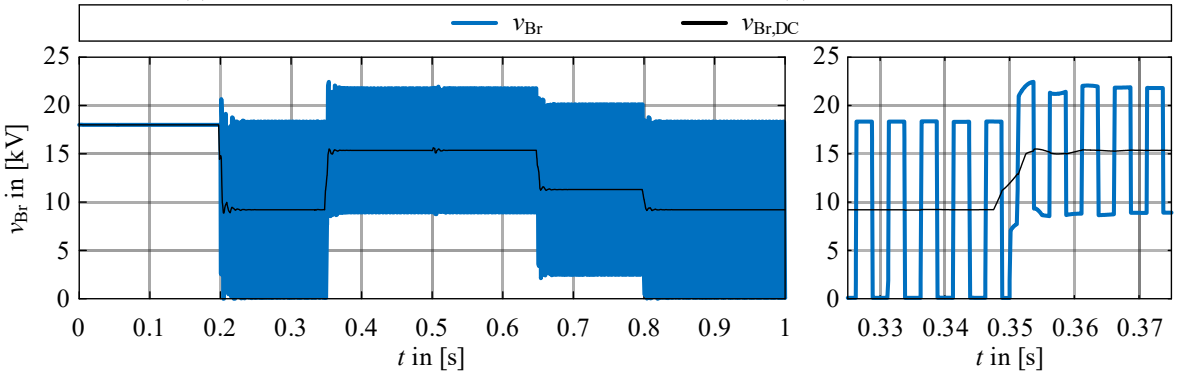

(e) Braking chopper: modulated arm voltage

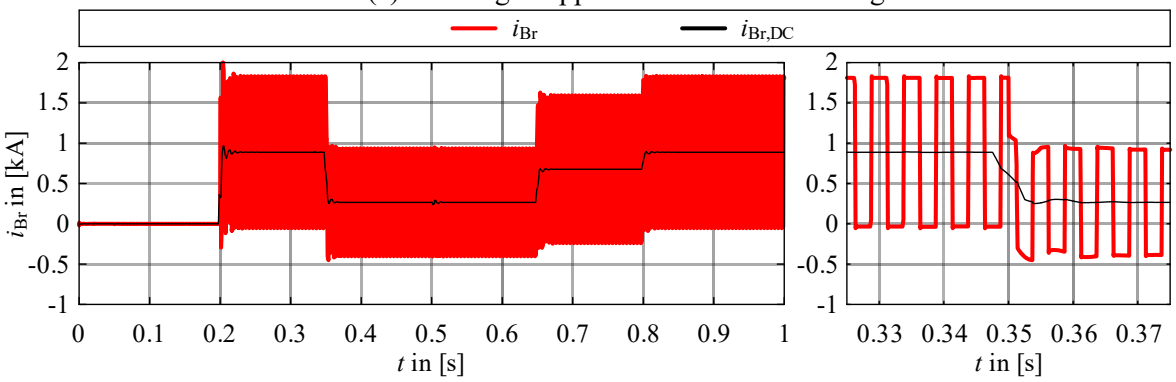

(f) Braking chopper: arm current

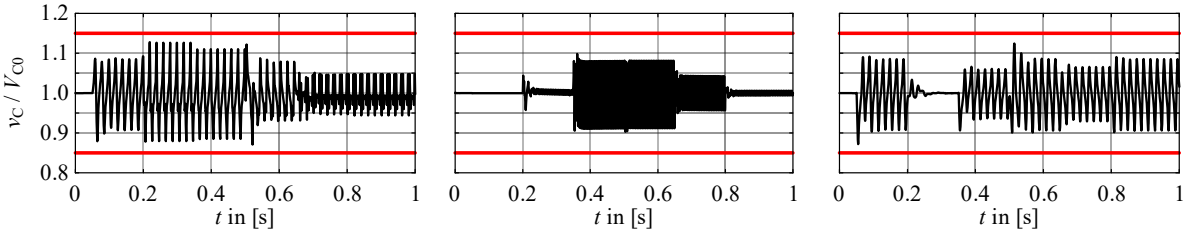

(g) Capacitor voltages MMC I (h) Capacitor voltages chopper (i) Capacitor voltages MMC II

Fig 11: Simulation results

Table I: Simulated operation sequence

	$P_{\mathrm{MMC,I}}$ [MW]	P_{BR} [MW]	$P_{\mathrm{MMC,II}}$ [MW]
t_1 = 0.05s	-16	0	16
t_2 = 0.20s	-16	16	0
t_3 = 0.35s	-16	4.8	11.2
t_4 = 0.50s	11.2	4.8	-16
t_5 = 0.65s	0	12.2	-12.2
t_6 = 0.80s	0	16	-16

The simulation starts in an idle mode. MMC I is voltage controlled and MMC II operates in current control mode. At $t = 50\mathrm{ms}$ a first load step is performed to $P_{\mathrm{MMC,I}} = -16\,\mathrm{MW}$ and $P_{\mathrm{MMC,II}} = 16\,\mathrm{MW}$. This represents a total power transfer from grid I to grid II. The Chopper is activated at $t = 200\mathrm{ms}$ and dissipates the total power. Consequently, no energy is transferred to MMC II leading to zero DC and AC currents (Fig. 11(b) and Fig. 11(d)). The chopper operates with a modulation frequency $f_{\mathrm{M}} = 200\,\mathrm{Hz}$. Due to the operation mode, the circulating chopper current is established between the braking chopper and MMC I. This leads to an increase of the capacitor voltages in this converter (Fig. 11(g)).

At $t = 350\mathrm{ms}$ the dissipated chopper power is reduced to $P_{\mathrm{Br}} = 4.8\,\mathrm{MW}$ and the remaining energy is transferred to MMC II. This operation point results in the biggest cell voltage ripple of the braking chopper (cf. Fig. 7(a)). At this point, the partial load factor is $a = 0.3$ and the energy ripple is $\Delta E_{\mathrm{Br}} = 20.4\,\mathrm{kJ}$, according to Fig. 7(a). Evaluating eq. (16), the considered system configuration and operation point leads to a voltage tolerance band $K_{\mathrm{T}} = 0.084$. That means, the voltage variation is $\pm 8.4\%$ in relation to the nominal capacitor voltage. That matches well with the simulation (Fig. 11(h)).

The load flow direction is reversed from MMC II to MMC I at $t = 500\mathrm{ms}$. At $t = 650\mathrm{ms}$ a further load step is performed to $P_{\mathrm{MMC,II}} = -12.2\,\mathrm{MW}$ and the total power is dissipated in the braking chopper. This represents a partial load factor $a = 0.76$. According to Fig. 7(a), this operation point halves the energy ripple, what is also in accordance to the simulation results.

Finally, the power rating is increased to $P_{\mathrm{MMC,II}} = -16\,\mathrm{MW}$ at $t = 800\mathrm{ms}$ and the chopper operates at nearly full load. The energy ripple is drastically reduced at this operation point. It can be seen that all requested points of operation are in a steady state mode in an appropriate time and the tolerance band is not exceeded, even during transient load steps. This shows the high flexibility of the considered operation method.

Conclusion

This paper investigates MMC based chopper topologies with a centralized resistor. It considers different cell configurations, such as half bridges, full bridges or a mix of both cell types. Furthermore, different modulation methods are analyzed. This paper presents a detailed description of the most relevant limiting factors and boundary conditions as well as the available degrees of freedom. Design and modulation optimizations are performed and it is shown that the trapezoidal modulation method is beneficial in comparison to sine-based modulations in many concerns. The HB chopper configuration should be used for common power ratings and provides an attractive solution with regard to system costs. The theoretical derivations are validated by a full-scale simulation model showing good correlation between the theoretical calculation and the generic system operation.

References

[1] R. Marquardt, “Modular Multilevel Converter: An universal concept for HVDC-Networks and DC-Bus-applications,” International Power Electronics Conference, pp. 502-507, 2010.

[2] M. Perez, S.Bernet, J. Rodriguez, S. Lizana and R. Kouro, “Circuit topologies, modelling, control schemes and applications of modular multilevel converters,” IEEE Trans. Power Electron., vol. 30, no. 1, pp. 4-17, 2015.

[3] M. Malinowski, K. Gopakumar, J. Rodriguez and M. Pérez, “A survey on Cascaded Multilevel Inverters,” IEEE Trans. Ind. Electron., vol. 57, no. 7, pp. 2197-2206, 2010.

[4] M. Glinka and R. Marquardt, “A New AC/AC Multilevel Converter Family,” IEEE Trans. Ind. Electron., vol. 52, no. 3, pp. 662-669, 2005.

[5] M. Hiller, D. Krug, R. Sommer, S. Rohner, “A new highly modular medium voltage converter topology for industrial drive applications,” IEEE EPE’09 ECCE Europe, pp. 1-10, 2009.

[6] A. Antonopoulos et al., “Modular multilevel converter AC motor drives with constant torque from zero to nominal speed,” IEEE Trans. Ind. App., vol. 50, no. 3, pp. 1982-1993, 2014.

[7] Y. Sun et al., “Predictive Power Control of Modular Multilevel Converter for Wind Energy Integration via HVDC,” IEEE PEDG 2020, pp. 334-339, 2020.

[8] R. Mourouvin et al., “AC/DC Dynamic Interactions of MMC-HVDC in Grid-Forming for Wind-Farm Intergration in AC Systems,” IEEE EPE’20 ECCE Europe, pp. 1-9, 2020.

[9] Y. Okazaki, S. Shioda and H. Akagi, “Performance of a Distributed Dynamic Brake for an Induction Motor Fed by a Modular Multilevel DSCC Inverter,” IEEE Trans. Power Electron., vol. 33, no. 6, pp. 4796-4806, 2018.

[10] M. Hagiwara, K. Nishimura and H. Akagi, “A medium-voltage motor drive with a modular multilevel PWM converter,” IEEE Trans. Power Electron., vol. 25, no. 7, pp. 1786-1799, 2010.

[11] P. Hofstetter, V. Hofmann and D. Karwatzki, “A detailed View on the Trapezoidal Operation for MMC Type Braking Chopper in Medium Voltage Applications,” IEEE EPE’ 22 ECCE Europe, p. 1-8, 2022.

[12] B. Xu et al., “A Novel DC Chopper Topology for VSC-Based Offshore Wind Farm Connection,” IEEE Trans. Pow. Electron., vol. 36, no. 3, 2021.

[13] J. Maneiro; S. Tennakoon; C. Barker and F. Hassan, “Energy diverting converter topologies for HVDC transmission systems,” IEEE EPE’13 ECCE Europe, pp.1-10, 2013.

[14] A. Birkel; A. Schön and M.-M. Bakran, " Analysis and semiconductor based comparison of energy diverting converter topologies for HVDC transmission systems,” IEEE EPE’17 ECCE Europe, pp. 1-10. 2017.

[15] V. Hofmann and M.-M. Bakran, “An Optimized Hybrid-MMC for HVDC,” Proc. PCIM Europe, pp. 1-8, 2016.

[16] A. Schön, A. Birkel and M.-M. Bakran, “Modulation and Losses of Modular Multilevel Converters for HVDC Applications,” Proc. PCIM Europe, 2014.